SCIENTIFIC REPORTS

OPEN

SUBJECT AREAS:
CHEMICAL ENGINEERING
DIVERSITY-ORIENTED SYNTHESIS
CARBON NANOTUBES AND FULLERENES
CATALYST SYNTHESIS

Received
30 April 2013

Accepted
23 December 2013

Published
22 January 2014

Correspondence and requests for materials should be addressed to K.H. (kenji-hata@aist.go.jp) or D.N.F. (d-futaba@aist.go.jp)

* These authors contributed equally to this work.

Diameter control of single-walled carbon nanotube forests from 1.3–3.0 nm by arc plasma deposition

Guohai Chen[1]*, Yasuaki Seki[1]*, Hiroe Kimura[1,2], Shunsuke Sakurai[1], Motoo Yumura[1], Kenji Hata[1,2,3] & Don N. Futaba[1]

[1]Nanotube Research Center, National Institute of Advanced Industrial Science and Technology (AIST), and Technology Research Association for Single Wall Carbon Nanotubes (TASC), Central 5, 1-1-1 Higashi, Tsukuba, Ibaraki 305-8565, Japan, [2]Department of Pure and Applied Sciences, Tsukuba University, Tsukuba, Ibaraki 305-8573, Japan, [3]Japan Science and Technology Agency (JST), Kawaguchi, Saitama 332-0012, Japan.

We present a method to both precisely and continuously control the average diameter of single-walled carbon nanotubes in a forest ranging from 1.3 to 3.0 nm with ~1 Å resolution. The diameter control of the forest was achieved through tuning of the catalyst state (size, density, and composition) using arc plasma deposition of nanoparticles. This 1.7 nm control range and 1 Å precision exceed the highest reports to date.

For single-walled carbon nanotubes (SWCNTs), the diameter represents a critical structural aspect as it determines many electronic and chemical properties. For instance, diameter determines the metallicity due to the inverse proportionality with the band gap[1]. Similarly, thermal properties are also dictated by the diameter as curvature is related with Umklapp scattering[2]. Finally, diameter determines the radius of curvature of the tube which affects surface functionalization[3]. Therefore, diameter represents an important structural parameter of SWCNTs; however, precise control of the SWCNT diameter over a wide range has yet to be demonstrated.

Previous results for the SWCNT diameter control can be grouped into two techniques: (1) floating catalyst method, where the SWCNTs are grown from catalysts flowing through a reactor tube, and (2) substrate growth, where the SWCNTs are grown from catalysts deposited onto a substrate. From our survey of previous reports, the floating catalyst method has demonstrated the widest range of SWCNT diameter control with the highest precision, particularly in the smaller diameter range (~<1 to ~2.1 nm)[4–6]. For example, Saito *et al.* demonstrated control from 1.2–1.8 nm with ~0.15 nm resolution by utilizing the differing activation temperatures of carbon sources[4]. Tian *et al.* controlled the diameter from 1.2–1.9 nm with a resolution of ~0.2 nm by controlling the CO_2 concentration[5]. The floating catalyst method affords this level of diameter control as the catalysts are not fixed in a single plane (*i.e.* the substrate) and therefore possess increased degrees of freedom to lessen the probability of aggregation.

For substrate growth, one basic approach has demonstrated the widest range of diameter control: increase catalyst spacing to minimize unwanted particle aggregation[7–11]. In this manner, Lu *et al.* reported diameter control of SWCNTs from 0.6 to 2.1 nm by selectively activating either the smaller or larger nanoparticles[7]. Durrer *et al.* used centrifugation method to separate the nanoparticles prior to deposition to control the diameter with a narrow distribution[8]. Song *et al.* achieved a narrow distribution of 0.1 nm with diameter control from 0.8 to 1.4 nm by using a sandwiched catalyst system[9]. Chen *et al.* controlled the diameter of CNTs from 0.9–1.8 nm by controlling the size of SiO_2 nanoparticles[10]. In each of these cases, the sparse distribution of nanoparticles (*i.e.* large catalyst spacing) was critical in reducing catalyst aggregation which resulted in entangled mats of SWCNTs.

When SWCNTs are efficiently grown from catalysts on a substrate, they self-organize into a vertically aligned assembly, called a "forest"[12–15]. However, the methods mentioned above do not grow in sufficient density to create a forest structure which is unique in several aspects. First, the forest represents a high efficiency and pure synthesis of CNTs from substrate-bound catalysts. Second, the forest structure cannot be formed at any other time than at the synthesis stage. Third, and most importantly, the forest structure provides a unique aligned structure for specialized processing, such as drawing CNT sheets and yarns[16–18] or aligned pre-impregnated composites[19]. Further, as the properties of a CNT depend on its structure, such as diameter, height, wall number, *etc*[20,21], several

reports have demonstrated that the properties of a forest also depend on the forest assembly structure, such as alignment[16,18,22,23]. Therefore, the ability to control the structure of the forest, in general, triggers advances in the application of CNTs, such as yarning[16,18], prepregs for composite reinforcement[19], viscoelastic materials[23], and thermal management materials[24], etc.

For SWCNT forests, sufficient catalyst density is required to create a condition where the non-self-supporting SWCNTs can self-organize into a vertically aligned ensemble through a "crowding effect"[25]. Arc plasma deposition (APD) is a physical nanoparticle deposition method where nanoparticles are generated in pulsed arc plasma from a target cathode at high voltages and allowed to deposit onto a substrate. This method possesses significant advantages over the conventional thin film catalyst systems commonly used to grow SWCNT forests. First, unlike thin film catalyst systems where the average nanoparticle size is determined by the film thickness, the size of nanoparticles can be easily controlled by adjusting the arcing voltage. Second, as nanoparticles are generated through an arc pulse, the number (*i.e.* density) of nanoparticles of a given size can be easily controlled by adjusting the pulse number. These two points allow for the independent control of nanoparticle size and density not allowable by the thin film catalyst system. Third, as the composition of the nanoparticles has been shown to agree (within 3%) with the target composition[26], APD allows for simple compositional changes to the catalyst. In previous reports, APD has been used to grow SWCNT, double-walled CNT, and multiwalled CNT (MWCNT) forests with diameters of 1.5, 4.0, and 5.5 nm, respectively, demonstrating that APD can make catalyst nanoparticles of different sizes[27].

In this paper, we have explored this opportunity to control the catalyst nanoparticle size and density, by which we realized the precise and continuous control of the average diameter of SWCNT forests from 1.3 to 3.0 nm with a resolution of ~1 Å. The control of catalyst size, density, and composition, which was carried out by tuning the APD power setting and target composition, was found to be critical in achieving wide range of diameter control to reduce catalyst aggregation. Finally, we found that the SWCNT forest height decreased with the average diameter, indicating that the synthesis of tall SWCNT forests with small diameter is inherently difficult.

Results

By the APD method, we were able to control the average diameter of SWCNT forests over a wide range (2.0 to 3.0 nm) with a precision of ~1 Å using Fe catalysts and grown by thermal chemical vapor deposition (CVD). This size control was achieved by the following strategy: At each APD power setting, which produced a specific size of nanoparticles, the pulse number was adjusted to achieve the sufficient nanoparticle density to allow the SWCNTs to self-assemble into a forest (Fig. 1a, see the detailed information in Supplementary Table S1 online). We should note that care was taken not to exceed this level too greatly as catalyst nanoparticle aggregation increased, which was particularly more prominent at the small diameter regime. We demonstrated the wide average diameter control of SWCNT forests from 2.0 to 3.0 nm with ~1 Å precision as shown by a series of Fourier transform infrared (FTIR) spectra (Fig. 1b). In short, the average diameter (d (nm)) was determined from the peak position of the S_{11} absorbance band and converted to diameter by the relation between binding energy and diameter ($d = 0.77/E$, where E (eV) is the peak position of S_{11} absorbance peak)[28]. Measurement reproducibility was confirmed by calculating the variance (~0.01 nm) of several measurements for a single sample. Measurement reproducibility due to processing was also confirmed by testing two other samplings taken from different areas of a single forest and found that the difference was ~0.01 nm. In fact, the standard deviation from the three locations was found only ~0.03 nm. These results demonstrated the high reproducibility and accuracy of this FTIR measurement. This method was applied to the family of SWCNT forests, and the family of FTIR spectra showed a clear and gradual upward shift in the S_{11} band associated with decreased diameter. To further support the FTIR measurements, diameter characterization by transmission electron microscopy (TEM) for ten members of the family of the SWCNT forests spanning the control range were performed, and the results agreed exceptionally well with FTIR results (Fig. 1c). Importantly, TEM observation also confirmed the 100% SWCNT selectivity as multi-shelled CNTs would not be detectable in the FTIR method.

As mentioned above, synthesizing SWCNT forests requires sufficient catalyst density so that SWCNTs can self-organize into a forest structure through a "crowding effect"[25]. This requirement of high catalyst density represents a fundamental obstacle for the SWCNT diameter control when synthesizing SWCNT forests with the conventional thin film catalyst, where the catalyst size and catalyst density are linked[29]. The APD method overcomes the limitation of the thin film catalyst system to simultaneously control the catalyst size and the sufficient catalyst density, which is particularly difficult at the smaller diameter regime. To demonstrate this point, four varieties of deposited nanoparticles showing size control were observed by atomic force microscopy (AFM), and these images showed the independent control of the particle size and density by the power setting (voltage) and discharge number (pulse number), respectively (Fig. 2). This aspect was critical to provide the required particle density for any particle size to drive the "crowding" of the individual SWCNTs into a self-assembled unit. Through this approach, we could control the diameter range from 2.0 to 3.0 nm using the Fe catalyst.

While the Fe catalyst offered a wide range of diameter control (2.0–3.0 nm), we found that the diameter range could be further extended by using alloyed Fe-Ni-Cr catalysts. This marks an additional advantage of APD where catalyst composition can be easily adjusted by the choice of target. We deposited nanoparticles of various sizes and densities for several Fe-Ni-Cr alloys to examine their limiting range (see Supplementary Table S1 online). Fe and Ni were chosen because of the high catalytic activity and carbon solubility for CNT synthesis. The major obstacle in controlling the diameter of CNTs, particularly for small diameter SWCNTs, is the migration of the catalyst material resulting in unwanted nanoparticle aggregation. To prevent or minimize this effect, Cr was chosen because the previous reports showed that it could suppress the catalyst migration by acting as spacer[30] or dispersant[31] between active catalysts or by reacting with the Al_2O_3 buffer layer to bind the catalyst nanoparticles[32]. After synthesis, the diameters were characterized and plotted as a function of each alloy in a ternary plot with colors representing the resulting SWCNT average diameters for forests, as shown in Fig. 3a. This ternary plot showed a strong dependence of the minimum diameter on the catalyst composition. Specifically, we observed that the increased Cr content resulted in the smaller diameter forests (as small as 1.3 nm) while the increased Ni content resulted in the larger diameter forests. It should be noted that we could not grow forest from 100% Ni catalysts at our growth conditions. To clarify the effect of the respective Ni and Cr content, we plotted the average SWCNT diameter as a function of Ni and Cr content shown in Figs. 3b and 3c, respectively. These plots showed the dependence of the lower achievable diameter range on the Ni and Cr content. Generally speaking, higher levels of Ni led to larger diameters, while higher levels of Cr led to smaller diameters. For practical purposes, we divided the entire diameter range into two regimes. In one regime, we used the Fe-Ni-Cr alloy catalyst to control the diameter in the small region (1.3–2.0 nm). In the second regime, we used the pure Fe catalyst for the large diameter SWCNTs (2.0–3.0 nm), as shown in Fig. 1b. Our results showed that tuning the catalyst condition (size, density, and composition) by APD was an effective method for controlling the average diameter of the SWCNTs in a forest where Cr was indispensable for extending the control range into the small diameter regime.

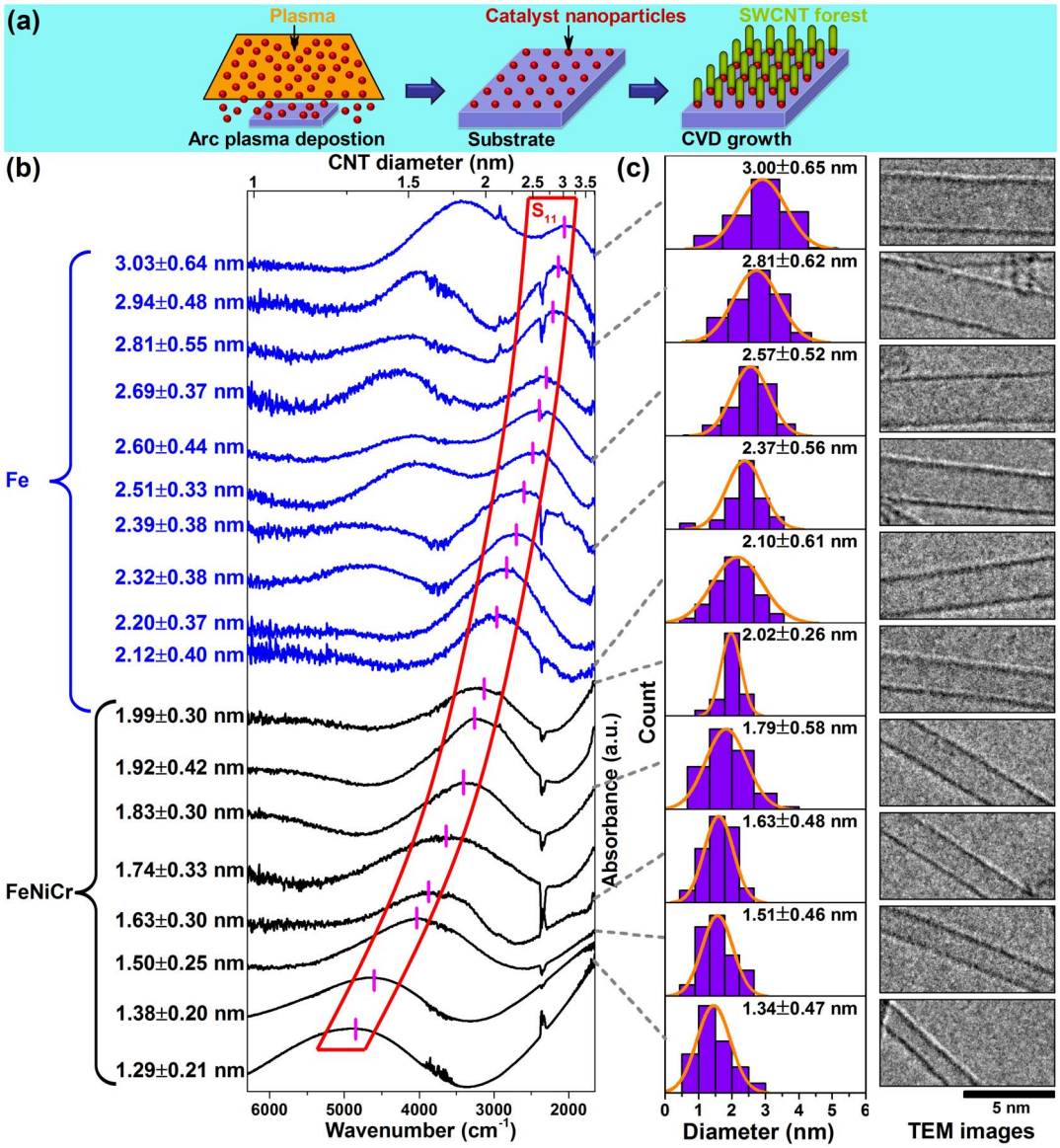

Figure 1 | Wide-range average diameter control of SWCNT forests. (a) Schematic of SWCNT forest growth with direct deposition of catalyst nanoparticles by APD. (b) Family of FTIR spectra demonstrating the wide-range average diameter control from 1.3 to 3.0 nm indicated by an upward shift in the S_{11} peak. (c) Diameter distribution histograms measured from TEM images confirming the average diameters obtained from the FTIR spectra, and the corresponding TEM images of representative SWCNTs.

Discussion

The results presented, herein, represent the widest range of average diameter control with the highest precision not only for SWCNT forests, but also for SWCNTs in general (Fig. 4). This level of diameter control in terms of range and precision rivals the highest reported levels and highlights our ability to control the structure of the SWCNT forests. From a literature survey, the floating catalyst method has demonstrated the widest and most precise control of SWCNT diameter (~<1 to ~2.1 nm)[4–6]. In addition, previous approaches, which used the sparse distribution of catalysts on substrates, have demonstrated a coarse control over a substantial diameter range[7–10]. Recently, the diameter control of SWCNT forests has also showed remarkable progress[33–37]. The mean diameter of SWCNT forests, spanning 1.2–2.5 nm, has been reported by changing both the relative and absolute amounts of Co and Mo in a binary catalyst system[34]. Further, the average diameter of SWCNTs was shown to reduce from 2.1 to 0.7 nm by the addition of acetonitrile to an ethanol carbon feedstock[35]. However, neither of these methods showed a fine diameter control. More recently, a report demonstrated the continuous and wide diameter range control of 1.9–3.2 nm of SWCNT forests by adjusting the catalyst formation temperature and the amount of hydrogen exposure for a thin film catalyst system to control Ostwald ripening and subsurface diffusion of the catalysts[36]. However, it should be noted that the APD method presented here possesses several advantages in both the results and approach. First, as the nanoparticles are generated independent of the CVD process, a large amount of hydrogen gas is not required. This is of particular importance when considering production costs and safety for mass production. Second, by using the flow rate control and the thin film catalyst, a strong dependence of the forest density and diameter was observed, while the APD method does not exhibit such a strong density dependence. This opens the opportunity to tune the forest structure for specific properties, such as higher porosity (lower density) or higher mechanical stiffness (higher density). Finally, our results demonstrate a wider control range of 1.3–3.0 nm, which is the widest level of control for the SWCNT average diameter in general. It is noteworthy to indicate that the forests produced in this study possess a broad diameter distribution. Sharp diameter distributions

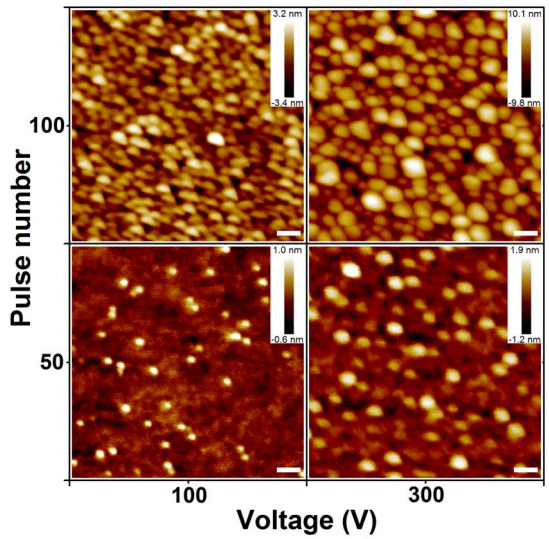

Figure 2 | **Demonstration of the independent control of the nanoparticle size and density of APD method, *i.e.* the nanoparticle size and density increase independently along with the voltage and pulse number, respectively. Scale bar: 50 nm.**

are not common in CVD methods, particularly in forests and/or on substrates. While post-processing separation techniques have shown extremely sharp diameter distributions and high resolutions[38–41], the disadvantage is the need for mono-dispersed SWCNTs and the low yield. Our method of the direct synthetic control shows much higher yield and wider diameter range despite the wider diameter distributions.

The widest range of diameter control of SWCNT forests was achieved by using Fe and Fe-Ni-Cr alloy catalysts, with Cr playing an important role in extending the control to smaller diameters. To further understand the effect of Cr, migration studies of the deposited catalysts were performed by AFM before and after identical thermal reduction processes for Fe and Fe-Ni-Cr alloy (SUS329J4L) catalyst nanoparticles. For Fe, the size of nanoparticles exhibited obvious increase after thermal annealing due to the Ostwald ripening (see Supplementary Fig. S1 online). In contrast, for Fe-Ni-Cr alloy, the catalyst nanoparticles showed a much smaller change in size and density, indicating that the presence of Cr suppressed the nanoparticle aggregation. The actual mechanism behind this remains uncertain, but a literature survey showed two different reports believed that Cr could act as spacer[30] or dispersant[31] between active catalysts. In a separate report, the Cr was thought to bind with the Al_2O_3 buffer layer to resist the migration[32]. It is our belief that the level of Cr in our study was insufficient to act as spacers; therefore, we attribute the suppression in aggregation to the binding to the Al_2O_3 buffer layer. As a result, by using alloyed Fe-Ni-Cr catalysts with

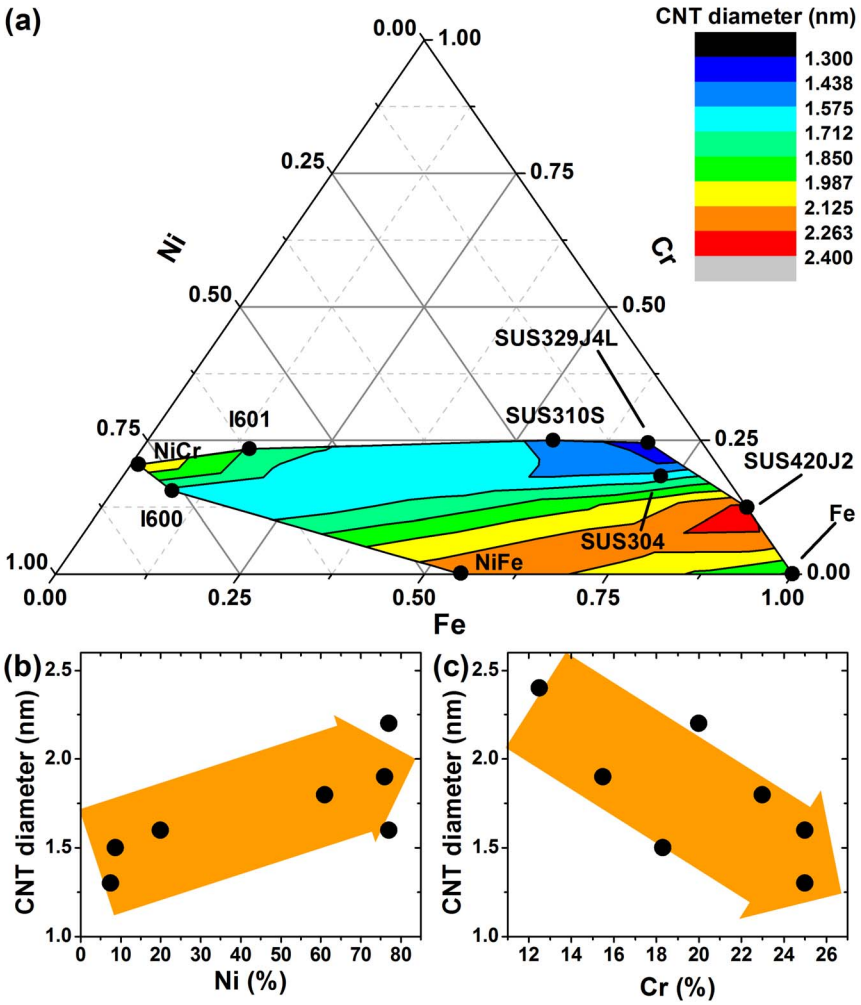

Figure 3 | (a) Ternary plot of the SWCNT average diameter as a function of the catalyst composition. Plots of the SWCNT average diameter as a function of (b) Ni and (c) Cr content (weight %). The arrows are just to guide the eyes.

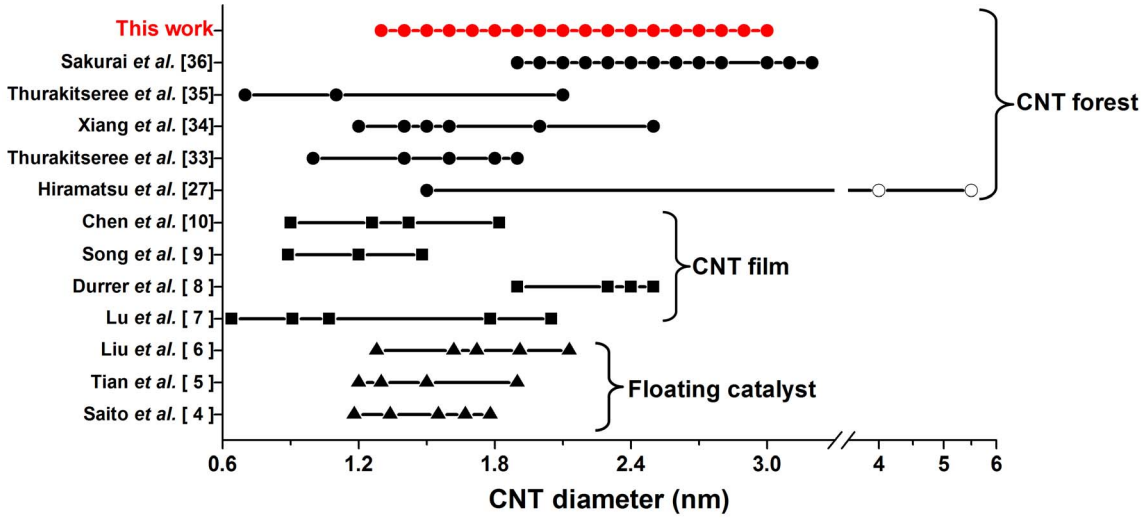

Figure 4 | Comparison of diameter range and size control of various SWCNTs. Data point and line indicate the precision and range, respectively. Triangle, rectangle, and circle indicate the floating catalyst method, CNT film, and CNT forest, respectively. Open circle indicates MWCNTs.

high-concentration of Cr, we were able to further extend the average diameter of SWCNT forests to small region.

The ability to precisely control the average diameter of SWCNT forests provides the opportunity to examine the dependence of the growth properties on the diameter. We plotted the height (achievable height in a fixed time) of our SWCNT forests as a function of the average diameter in Fig. 5, which showed that the height decreased with decreased diameter. Specifically, for the larger diameter range, ~2.8–3.0 nm, the forest was highest, ~300–500 μm, under these growth conditions, as shown in the upper right inset scanning electron microscopy (SEM) image of Fig. 5; however, for the medium diameter range, ~2.2–2.6 nm, the forest height dropped to about half (~100–200 μm). Finally, the forest height for ~1.3–1.6 nm fell to several tens of μm. These results may explain the absence of long length and small diameter SWCNT forests. Our results are completely the opposite trend reported by Patole *et al.* where smaller particles, due to their smaller surface area and volume, would grow CNTs at faster growth rates (height per growth time)[42]. We suggest the most plausible reason is that the effect of gas diffusion becomes an increasingly greater effect as the diameter is reduced. As stated previously, one requirement for SWCNT forest growth is a critical catalyst density to create sufficient crowding among the SWCNTs so as to form the forest and this critical density increases with decreased diameter[25]. By calculating the inter-tube spacing from the linear mass density (mass per unit length) of the average diameter and bulk mass density[43], the inter-tube spacing for the 1.3-nm-diameter forests was ~1/3 of that for the 3.0-nm-diameter forests (*i.e.* ~5.4 nm versus ~13.6 nm, see Supplementary Table S1 online). A recent report on

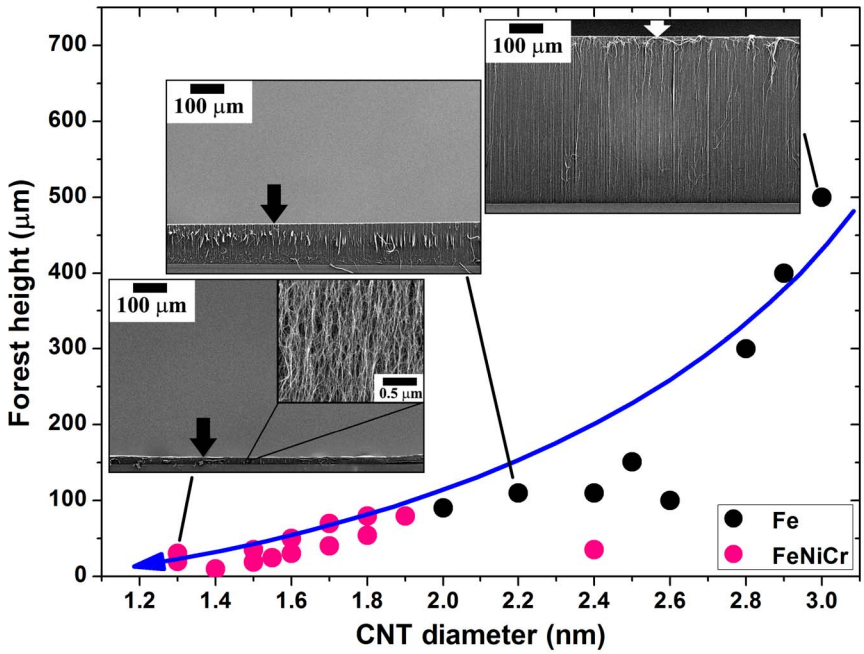

Figure 5 | Height of SWCNT forests as a function of the average diameter with color-coded for catalyst type. The blue curved arrow is to guide the eyes. The insets of SEM images demonstrate the decreased height along with the decreased diameter. The arrows in SEM images indicate the very top of the SWCNT forests.

CVD synthesis of CNTs concluded that gas diffusion occurred in the Knudsen diffusion regime, and the effective Knudsen diffusivity was proportional to the channel radius (*i.e.* the inter-tube spacing in this work) and the porosity of the forest, and inversely proportional to the tortuosity factor, at a fixed temperature[44]. As stated, the channel radius was ~1/3 for the smaller diameter CNTs, but the calculated porosity of these two forests was nearly the same (~97%). We estimated that the effective Knudsen diffusivity for the small diameter (1.3 nm) forests was at least 1/3 lower than that of the large diameter (3.0 nm) forests. We expect this value (1/3) to be an upper limit as the tortuosity factor of a forest of small diameter and flexible SWCNTs is expected to be higher than one of larger diameter and stiffer SWCNTs. Therefore, we conclude that difference in gas diffusion is one potential cause of the observed decreased height of forests with diameter. This explains the apparent difference between our results and that of Patole *et al.*, where the inter-tube spacing was significantly larger and diffusion was not a major factor[42]. Another reason for the height decrease with diameter could be based on recent findings that the mass of the individual SWCNT is determined by the individual catalyst volume, and consequently the forest yield is determined by the total catalyst volume[36,45]. This implies that larger diameter SWCNTs will provide larger length whereas smaller diameter SWCNTs will provide shorter length. Finally, due to the addition of low carbon solubility element, Cr, into the Fe catalyst nanoparticles, we would expect an overall decrease in carbon solubility. This decreased carbon solubility may explain not only the diminishing height of forests even after the optimization of CVD conditions but also the slower growth rates. Therefore, our results suggest that the synthesis of tall SWCNT forests with small diameter is inherently difficult.

To summarize, this work demonstrated the precise and continuous control of SWCNT average diameter in a forest ranging from 1.3 to 3.0 nm with ~1 Å resolution by using APD of catalyst nanoparticles. Through APD, the catalyst condition (size, density, and composition) was tuned and shown as an effective method for controlling the SWCNTs in a forest where Cr led to smaller diameters and Ni led to larger diameters. Our results represent the widest range of the average diameter control with the highest precision for SWCNTs in general. Investigation of the growth properties showed a direct relationship between the achievable height and the diameter suggesting the fundamental difficulty in synthesizing tall and small diameter SWCNT forests.

Methods

Catalyst deposition. Catalyst nanoparticles were deposited by APD in a high vacuum chamber ($\sim 4 \times 10^{-4}$ Pa) onto silicon substrates with a 40 nm thick sputtered Al_2O_3 buffer layer. Deposition parameters included the voltage and pulse number (see Supplementary Table S1 online). Voltage, determining arc current, was increased to increase nanoparticle size and ranged from 80–180 V at a fixed capacitance of 720 μF. The density of deposited nanoparticles was determined by the number of arc pulses, which ranged from 100 to 170.

Synthesis. SWCNT forests were synthesized in a 1″ tube furnace by thermal CVD using helium as the carrier gas and 1% ethylene as the carbon source at 1000 sccm total flow. Catalyst aggregation was minimized by reducing the accumulated heat exposure to the catalyst nanoparticles. Specifically, the 1 × 1 cm silicon substrate was inserted into a preheated CVD system (750°C) to reduce the metallic nanoparticles (90% hydrogen in helium) for 1 min, immediately followed by a growth phase for 6 min. In our previous reports we added water to increase the height of forests[14]. However, in this study, we have not added water as it increased the average diameter of SWCNTs. Therefore, the CVD conditions for the data presented herein were fixed for simplicity.

Characterization. The catalyst nanoparticles were observed by AFM (BRUKER Dimension FastScan). The forest structures were characterized by SEM (Hitachi S-4800). The average diameter of SWCNTs was analyzed by FTIR spectroscopy (Nicolet 6700). Diameter evaluation by FTIR is based on the conversion of the peak of the S_{11} absorption band to diameter by the relation between SWCNT diameter and binding energy (*i.e.* Kataura plot)[28]. In this method, a sample of SWCNTs was removed from the forest and dispersed in organic solvent, such as ethanol, dimethylformamide, etc. and then dropped onto a stainless steel mesh and dried. Transmission FTIR spectroscopy was performed, and the location of the S_{11} absorption band (E (eV)) was converted to diameter (d (nm)) by the following relation, $d = 0.77/E$, which was derived simply from the Kataura plot. It should be noted that while the shape of the FTIR absorption peak is dependent on the SWCNT dispersion, the peak position is highly consistent. Finally, the FTIR results were confirmed by TEM (TOPCON EM-002B) observation.

1. Wildöer, J. W. G., Venema, L. C., Rinzler, A. G., Smalley, R. E. & Dekker, C. Electronic structure of atomically resolved carbon nanotubes. *Nature* **391**, 59–62 (1998).
2. Yu, C. H., Shi, L., Yao, Z., Li, D. Y. & Majumdar, A. Thermal conductance and thermopower of an individual single-wall carbon nanotube. *Nano Lett.* **5**, 1842–1846 (2005).
3. Strano, M. S. *et al.* Electronic structure control of single-walled carbon nanotube functionalization. *Science* **301**, 1519–1522 (2003).
4. Saito, T., Ohmori, S., Shukla, B., Yumura, M. & Iijima, S. A novel method for characterizing the diameter of single-wall carbon nanotubes by optical absorption spectra. *Appl. Phys. Express* **2**, 095006 (2009).
5. Tian, Y. *et al.* Tailoring the diameter of single-walled carbon nanotubes for optical applications. *Nano Res.* **4**, 807–815 (2011).
6. Liu, Q. F. *et al.* Diameter-selective growth of single-walled carbon nanotubes with high quality by floating catalyst method. *ACS Nano* **2**, 1722–1728 (2008).
7. Lu, C. G. & Liu, J. Controlling the diameter of carbon nanotubes in chemical vapor deposition method by carbon feeding. *J. Phys. Chem. B* **110**, 20254–20257 (2006).
8. Durrer, L. *et al.* Narrowing SWNT diameter distribution using size-separated ferritin-based Fe catalysts. *Nanotechnology* **20**, 355601 (2009).
9. Song, W. *et al.* Synthesis of bandgap-controlled semiconducting single-walled carbon nanotubes. *ACS Nano* **4**, 1012–1018 (2010).
10. Chen, Y. B. & Zhang, J. Diameter controlled growth of single-walled carbon nanotubes from SiO_2 nanoparticles. *Carbon* **49**, 3316–3324 (2011).
11. Chiang, W. H. & Sankaran, R. M. Linking catalyst composition to chirality distributions of as-grown single-walled carbon nanotubes by tuning Ni_xFe_{1-x} nanoparticles. *Nat. Mater.* **8**, 882–886 (2009).
12. Ren, Z. F. *et al.* Synthesis of large arrays of well-aligned carbon nanotubes on glass. *Science* **282**, 1105–1107 (1998).
13. Fan, S. S. *et al.* Self-oriented regular arrays of carbon nanotubes and their field emission properties. *Science* **283**, 512–514 (1999).
14. Hata, K. *et al.* Water-assisted highly efficient synthesis of impurity-free single-walled carbon nanotubes. *Science* **306**, 1362–1364 (2004).
15. Murakami, Y. *et al.* Growth of vertically aligned single-walled carbon nanotube films on quartz substrates and their optical anisotropy. *Chem. Phys. Lett.* **385**, 298–303 (2004).
16. Zhang, M., Atkinson, K. R. & Baughman, R. H. Multifunctional carbon nanotube yarns by downsizing an ancient technology. *Science* **306**, 1358–1361 (2004).
17. Zhang, M. *et al.* Strong, transparent, multifunctional, carbon nanotube sheets. *Science* **309**, 1215–1219 (2005).
18. Jiang, K. L., Li, Q. Q. & Fan, S. S. Nanotechnology: Spinning continuous carbon nanotube yarns - Carbon nanotubes weave their way into a range of imaginative macroscopic applications. *Nature* **419**, 801 (2002).
19. Kobashi, K. *et al.* Epoxy composite sheets with a large interfacial area from a high surface area-supplying single-walled carbon nanotube scaffold filler. *Carbon* **49**, 5090–5098 (2011).
20. Ebbesen, T. W. *et al.* Electrical conductivity of individual carbon nanotubes. *Nature* **382**, 54–56 (1996).
21. Fujii, M. *et al.* Measuring the thermal conductivity of a single carbon nanotube. *Phys. Rev. Lett.* **95**, 065502 (2005).
22. Qu, L. T., Dai, L. M., Stone, M., Xia, Z. H. & Wang, Z. L. Carbon nanotube arrays with strong shear binding-on and easy normal lifting-off. *Science* **322**, 238–242 (2008).
23. Xu, M., Futaba, D. N., Yamada, T., Yumura, M. & Hata, K. Carbon nanotubes with temperature-invariant viscoelasticity from −196° to 1000°C. *Science* **330**, 1364–1368 (2010).
24. Huang, H., Liu, C. H., Wu, Y. & Fan, S. S. Aligned carbon nanotube composite films for thermal management. *Adv. Mater.* **17**, 1652–1656 (2005).
25. Xu, M., Futaba, D. N., Yumura, M. & Hata, K. Alignment control of carbon nanotube forest from random to nearly perfectly aligned by utilizing the crowding effect. *ACS Nano* **6**, 5837–5844 (2012).
26. Cai, C. L., Wang, J. M., Yan, Y. X., Hang, L. X. & Zhu, C. Nickel-chrome-iron alloy film deposited by pulsed arc deposition. *IEEE Trans. Plasma Sci.* **30**, 725–727 (2002).
27. Hiramatsu, M., Deguchi, T., Nagao, H. & Hori, M. Aligned growth of single-walled and double-walled carbon nanotube films by control of catalyst preparation. *Jpn. J. Appl. Phys.* **46**, L303–L306 (2007).
28. Kataura, H. *et al.* Optical properties of single-wall carbon nanotubes. *Synth. Met.* **103**, 2555–2558 (1999).
29. Zhao, B. *et al.* Exploring advantages of diverse carbon nanotube forests with tailored structures synthesized by supergrowth from engineered catalysts. *ACS Nano* **3**, 108–114 (2009).
30. Shimoi, N. & Tanaka, S. Enhancement of electron field emission from carbon nanofiber bundles separately grown on Ni catalyst in Ni-Cr alloy. *Carbon* **47**, 1258–1263 (2009).

31. Chen, B. & Wu, P. Aligned carbon nanotubes by catalytic decomposition of C_2H_2 over Ni-Cr alloy. *Carbon* **43**, 3172–3177 (2005).
32. Mattevi, C. *et al.* In-situ X-ray photoelectron spectroscopy study of catalyst-support interactions and growth of carbon nanotube forests. *J. Phys. Chem. C* **112**, 12207–12213 (2008).
33. Thurakitseree, T. *et al.* Diameter controlled chemical vapor deposition synthesis of single-walled carbon nanotubes. *J. Nanosci. Nanotechnol.* **12**, 370–376 (2012).
34. Xiang, R. *et al.* Diameter modulation of vertically aligned single-walled carbon nanotubes. *ACS Nano* **6**, 7472–7479 (2012).
35. Thurakitseree, T. *et al.* Diameter-controlled and nitrogen-doped vertically aligned single-walled carbon nanotubes. *Carbon* **50**, 2635–2640 (2012).
36. Sakurai, S., Inaguma, M., Futaba, D. N., Yumura, M. & Hata, K. Diameter and density control of single-wall carbon nanotube forests by modulating Ostwald ripening through decoupling the catalyst formation and growth processes. *Small* **9**, 3584–3592 (2013).
37. Chen, G. H. *et al.* Absence of an ideal single-walled carbon nanotube forest structure for thermal and electrical conductivities. *ACS Nano* **7**, 10218–10224 (2013).
38. Arnold, M. S., Green, A. A., Hulvat, J. F., Stupp, S. I. & Hersam, M. C. Sorting carbon nanotubes by electronic structure using density differentiation. *Nat. Nanotechnol.* **1**, 60–65 (2006).
39. Bonaccorso, F. *et al.* Density gradient ultracentrifugation of nanotubes: Interplay of bundling and surfactants encapsulation. *J. Phys. Chem. C* **114**, 17267–17285 (2010).
40. Tu, X. M., Manohar, S., Jagota, A. & Zheng, M. DNA sequence motifs for structure-specific recognition and separation of carbon nanotubes. *Nature* **460**, 250–253 (2009).
41. Ghosh, S., Bachilo, S. M. & Weisman, R. B. Advanced sorting of single-walled carbon nanotubes by nonlinear density-gradient ultracentrifugation. *Nat. Nanotechnol.* **5**, 443–450 (2010).
42. Patole, S. P. *et al.* Kinetics of catalyst size dependent carbon nanotube growth by growth interruption studies. *Appl. Phys. Lett.* **96**, 094101 (2010).
43. Futaba, D. N. *et al.* 84% catalyst activity of water-assisted growth of single walled carbon nanotube forest characterization by a statistical and macroscopic approach. *J. Phys. Chem. B* **110**, 8035–8038 (2006).
44. Zhu, L. B., Hess, D. W. & Wong, C. P. Monitoring carbon nanotube growth by formation of nanotube stacks and investigation of the diffusion-controlled kinetics. *J. Phys. Chem. B* **110**, 5445–5449 (2006).
45. Sakurai, S., Inaguma, M., Futaba, D. N., Yumura, M. & Hata, K. A fundamental limitation of small diameter single-walled carbon nanotube synthesis - A scaling rule of the carbon nanotube yield with catalyst volume. *Materials* **6**, 2633–2641 (2013).

Acknowledgments

Support by Technology Research Association for Single Wall Carbon Nanotubes (TASC) is acknowledged.

Author contributions

G.C. and Y.S. designed and conducted the experiments. H.K. and S.S. helped with the experiment equipment. K.H. and D.N.F. supervised the overall research. G.C., Y.S. and D.N.F. drafted the paper. M.Y. guided this work. All authors read and commented on the manuscript.

Additional information

Supplementary information accompanies this paper at http://www.nature.com/scientificreports

Competing financial interests: The authors declare no competing financial interests.

How to cite this article: Chen, G.H. *et al.* Diameter control of single-walled carbon nanotube forests from 1.3–3.0 nm by arc plasma deposition. *Sci. Rep.* **4**, 3804; DOI:10.1038/srep03804 (2014).